ACS APPLIED MATERIALS & INTERFACES

Research Article

www.acsami.org

Matrix-Assisted Three-Dimensional Printing of Cellulose Nanofibers for Paper Microfluidics

Sungchul Shin[†] and Jinho Hyun*[,†,‡,§]

[†]Department of Biosystems and Biomaterials Science and Engineering, [‡]Research Institute of Agriculture and Life Sciences, and [§]Center for Food and Bioconvergence, Seoul National University, Seoul 151-921, Republic of Korea

Supporting Information

ABSTRACT: A cellulose nanofiber (CNF), one of the most attractive green bioresources, was adopted for construction of microfluidic devices using matrix-assisted three-dimensional (3D) printing. CNF hydrogels can support structures printed using CAD design in a 3D hydrogel environment with the appropriate combination of rheological properties between the CNF hydrogel and ink materials. Amazingly, the structure printed freely in the bulky CNF hydrogels was able to retain its highly resolved 3D features in an ultrathin two-dimensional (2D) paper using a simple drying process. The dimensional change in the CNF hydrogels from 3D to 2D resulted from simple dehydration of the CNFs and provided transparent, stackable paper-based 3D channel devices. As a proof of principle, the rheological properties of the CNF hydrogels, the 3D structure of the ink, the formation of channels by evacuation of the ink, and the highly localized selectivity of the devices are described.

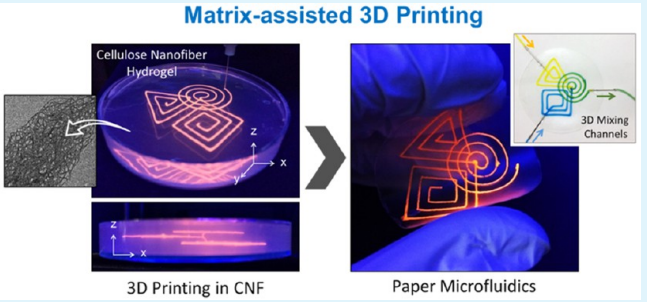

KEYWORDS: *cellulose nanofiber, matrix-assisted 3D printing, 3D open-channel microfluidic devices, hydrogel, dimensional change*

1. INTRODUCTION

The current major problems in three-dimensional (3D) printing are focused on inks and printing systems. However, in addition to ink, the matrix is one of the most critical components in 3D printing of soft matter. Nevertheless, matrix research is rarely reported due to the lack of selectable materials. The matrix plays an important role in maintaining printed structures in a free-standing form in the bulk space.[1,2] To this end, the simple removal of ink from the matrix enabling the construction of microchannels became the starting point of the research on matrix-assisted 3D printing of microfluidic devices. In addition, the deformation of a bulky matrix into a film enforced the vertical integration of 3D structures by natural dehydration, and it made the research more challenging.

Extrusion 3D printing using a matrix and ink was most effective for printing free-standing structures and a smart choice for the rapid prototyping of microfluidic systems due to the ease of processing and freedom of design. The free-standing 3D structures could be fabricated by extruding inks in the liquid matrix including PDMS prepolymers,[3,4] self-healing hydrogels,[5] and granular gel media.[6] We adopted a green material, a cellulose nanofiber (CNF) hydrogel, as a potential novel matrix in this research, and the critical factors were investigated for the 3D printing of free-standing structures using this material.

Cellulose is a limitless resource on earth, and CNFs have been widely researched from a new angle in recent decades. Because of a high water content of 98% and superior mechanical properties,[7,8] CNFs have been applied as substrates for transparent films,[9−12] porous packaging,[13] tissue engineering scaffolds,[14−16] hydrogels and aerogels,[17−19] and battery electrodes.[20−22] In recent years, CNFs have been used as an additive to ink for the enhancement of low viscosity in the ink, for the directional deformation of structures, and as an embedding material for direct 3D printing.[23−26] However, to the best of our knowledge, no research has been reported on the use of CNFs as a matrix in 3D printing or a platform for microfluidic devices.

In our research, it was possible to print microfluidic channels using a CNF hydrogel matrix in a simple and rapid process. The vertical integration of the microchannels printed in three-dimensions was achieved through simple drying. This is a unique new concept in fabrication of microfluidic systems that has not yet been reported. The bulky CNF hydrogel matrix deformed into a thin film during drying. Since a thin and dense barrier of CNF was formed between the printed features, the resolved integration of microchannels was naturally achieved.

CNF hydrogels are composed of high aspect ratio natural nanofibers; CNF films with microchannels are flexible and even foldable after dehydration, and additional selective finishing processes were available. In addition, it was possible to monitor the chemical reactions in the microchannels due to the high transparency of CNF-based devices fabricated by matrix-assisted 3D printing. Another unique feature of our microfluidic devices is that they are distinct from paper-wicking sensing

Received: May 29, 2017
Accepted: July 24, 2017
Published: July 24, 2017

DOI: 10.1021/acsami.7b07609
ACS Appl. Mater. Interfaces XXXX, XXX, XXX−XXX

platforms, which suffer from undesirable retention, high adsorption of analytes to the bulk, and the opacity of paper.[27−30]

This is the first report to fabricate microfluidic channels in the CNF matrix using 3D printing and to integrate the 3D structures by deforming the matrix to two dimensions. It will be applicable to the compact design of microfluidic devices and the effective stacking of multitasking devices by simply connecting the layers. With a simple process and easy control of the composition, a CNF hydrogel could be used as a generic matrix for 3D printing with the combination of a variety of ink materials in the future.

2. EXPERIMENTAL SECTION

2.1. Preparation of a CNF Hydrogel Matrix. A CNF hydrogel matrix was produced from craft pulp (Moorim P&P, Ulsan, Korea). Prior to carboxymethylation and nanofibrillation, the pulp fibers were beaten using a laboratory valley beater for 30 min. Beaten pulp fibers were carboxymethylated, and the procedure was summarized as follows. The wet pulp (dry weight, 70 g) was solvent-exchanged using a series of graded ethanol solutions (50%, 70%, 90%, and 100%) with centrifugation at 12 000 rpm for 5 min. The solvent-exchanged pulp fiber was immersed in a solution of monochloroacetic acid (14 g, Sigma-Aldrich, St Louis, MO, USA) in isopropanol (3200 mL)/methanol (800 mL) for 30 min. A solution of methanol (250 mL) and isopropanol (1000 mL) with sodium hydroxide (11.2 g) was added to the cellulose slurry, and the mixture was heated at 65 °C under continuous stirring for 60 min. This carboxymethylated cellulose fiber was solvent-exchanged using distilled water to pH 7.0 and passed through a grinder (Super Masscolloider, Masuko Sangyo Co., Ltd., Japan) to produce the CNF hydrogel. The consistency of the pulp suspension during grinding was 1.5 w/v %. The operation speed and the gap distance between the grinder stones were 1500 rpm and −100 μm, respectively. The number of passes through the grinder was fixed at five. After grinding, the CNFs were diluted to 0.3 w/v % and tip-sonicated at 50% amplitude for 30 min. To remove the remaining microscale cellulose fibers, the sonicated cellulose suspension was centrifuged at 20 000 rpm for 10 min. The supernatant was collected and concentrated to produce 0.4−1.0 w/v % CNF hydrogel matrices.

2.2. Preparation of the Removable Petroleum-Jelly-Based Ink. The removable ink for matrix-assisted 3D printing was prepared by mixing petroleum jelly (Sigma-Aldrich) and liquid paraffin (Sigma-Aldrich) at three ratios (10:0, 7.5:2.5, and 5:5). The mixed inks were heated to 70 °C, vigorously stirred for 1 min, and degassed in a planetary centrifugal mixer. To visualize the embedded printing, 0.1 wt % fluorescent microparticles was added to the petroleum-jelly inks.

2.3. Measurement of the Rheological Properties of the CNF Matrices and the Inks. The rheological behavior of the CNF hydrogel matrix and the removable ink was characterized using a digital rheometer (MARSIII, ThermoScientific, Newington, NH, USA) fitted with a parallel plate geometry (35 mm radius) to investigate shear-thinning properties. Prior to rheological characterization, the CNF hydrogel matrix and the removable ink were vigorously stirred and degassed with a centrifuge at 1000 rpm and 4000 rpm, respectively. Rheological measurements were obtained for the matrix and the inks within 20 min of their preparation. Various concentrations of CNF hydrogels were placed in the plate and subjected to stress-sweep experiments, employing a stress range from 0.1 to 1000 Pa at a frequency of 1 Hz at 25 °C. The shear viscosity of the matrix and the inks was obtained at 25 °C, and the measurement was performed in Rot Ramp mode at shear rates from 0.01 to 1000 s^{-1} with a gap size of 1.0 mm. Stress sweeps from 0.1 to 1000 Pa at a frequency of 1 Hz were performed at 70 °C to define the shear modulus change of the petroleum-jelly inks.

2.4. Matrix-Assisted 3D Printing. The 3D patterns were produced by printing petroleum-jelly ink in a CNF hydrogel matrix using a custom-built 3D printer. The 3D patterns were designed using the commercially available Rhinoceros software (Rhinoceros 5.0, Robert McNeel & Associates, Seattle, WA, USA). The designed 3D models were translated into G-code instructions for the deposition stage using 3D-printing slicing software (Cura, Ultimaker, Geldermalsen, Netherlands). All printing paths were generated by writing the appropriate G-code commands. Prior to printing the path designs, the CNF hydrogel matrix was poured into a Petri dish at 25 °C. The melted petroleum-jelly ink at 70 °C was poured into the syringe and cooled to 25 °C for 3 h before printing. The nozzle tip was inserted into the bottom center of the CNF hydrogel matrix in the Petri dish, and the G-code was sent to the printer using the host software. The ink was extruded through a 160 μm inner diameter nozzle installed in a 5 mL syringe. The extruding volume and the thickness of the lines were controlled with applied pressure and printing speed. The concentration of the CNF matrix was varied from 0.4 to 1.0 w/v %, and the ratio of petroleum jelly/liquid paraffin was varied to 1.0, 0.75, and 0.5 to determine the optimal condition for printing.

2.5. Fabrication of 3D Open-Channel Microfluidic Devices. The 3D open channels were fabricated by removing the inks from the CNF matrix printed with the petroleum-jelly ink after drying. For the removal of the petroleum-jelly inks, the 3D structures embedded in the CNF matrix were heated to 70 °C in the oven for 5 min. The melted ink was removed by applying compressed air through the channels, and the inner surface of the channels was washed with *n*-hexane several times by flowing it through the channels at 70 °C. The conversion of the hydrophilic CNF channel surface to a hydrophobic state was achieved using 10 wt % trimethylchlorosilane in *n*-hexane with continuous flowing of the solution. After silanization, the inner channel surface was coated with silicone elastomer (SH 9555, Dow Corning, Midland, MI, USA). The silicone elastomer base was mixed with a curing agent at a 20:1 weight ratio, and the solution was diluted to 30 wt % with *n*-hexane. The dilute solution of silicone elastomer was spread on the inner channel surface and was cured for 10 min at 80 °C. A silicone elastomer solution containing 0.1% fluorescent polystyrene microspheres (2 μm, yellow-green FluoSpheres, Invitrogen, Eugene, OR, USA) was used to visualize the specific layer of silicone elastomer cured at the inner channel surface. Lines of printed ink were imaged using fluorescence optical microscopy (Olympus BX51, Tokyo, Japan). The surface morphology and the cross section of the 3D multichannel were imaged using field-emission scanning electron microscopy (FE-SEM, SUPRA 55VP, Carl Zeiss, Oberkochen, Germany) at an operation voltage of 2 keV. Platinum was sputtered onto the cross-sectional area of the microfluidic devices at 20 mV for 160 s as a conductive coating for imaging purposes. The surface topography of the inner channel surface was imaged using atomic force microscopy (AFM, XE100, Park Systems, Suwon, Korea) in a noncontact mode (PPP-NCHR 10M, Nanosensors, Neuchâtel, Switzerland) at the scan rate of 0.6 Hz for surface areas of 2 × 2 μm^2.

2.6. pH-Sensitive Colorimetric Analysis. A CNF microfluidic device was printed with petroleum-jelly ink according to the CAD design with coiled detection zones. Prior to removing the inks, a universal pH indicator was dropped onto a coiled feature. After additional drying, the CNF film with printed structures was detached from the Petri dish, and the petroleum-jelly ink was removed by flowing *n*-hexane through the channels at 70 °C. The inner surface of the microchannels was not coated with silicon elastomer, and distilled water (DW), 1 M NaOH, and 1 M HCl were injected into the channel sequentially. The colorimetric changes at the detection zone were captured with a digital camera.

2.7. Selective Detection of Chromium and Nickel Ions. A CNF microfluidic device with three inlets, mixing zones, and detection zones was 3D-printed with petroleum-jelly ink according to the CAD design. The petroleum-jelly ink was removed from the channels, whose inner surface was coated with silicon elastomer, except for the detection zones. Then, 0.01 M dimethylglyoxime (Sigma-Aldrich) was dissolved in an ethanol/water (60/40) solution for the detection of nickel ions, and 0.01 M 1,5-diphenylcarbazide (Sigma-Aldrich) was dissolved in acetone/water (60/40) solution for the detection of chromium ions. The dimethylglyoxime and 1,5-diphenylcarbazide solutions were dropped onto the allocated detection zones and were dried completely at 70 °C for 1 h. Different concentrations of

DOI: 10.1021/acsami.7b07609
ACS Appl. Mater. Interfaces XXXX, XXX, XXX−XXX

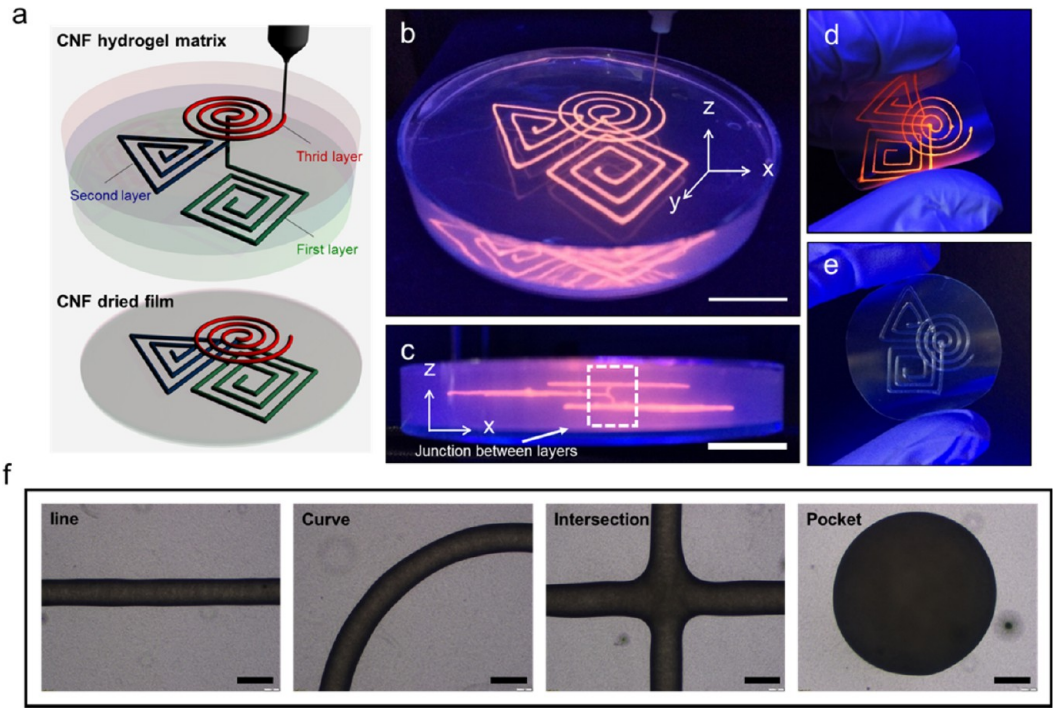

Figure 1. Fabrication of a flexible microfluidic thin film with multilayered channels by matrix-assisted 3D printing in the CNF hydrogel. (a) Series of fabrication processes for three-layered continuous microfluidic channels designed by CAD. (b) Nozzle tip was moved to the three layers, and the petroleum-jelly-based removable ink was injected in the CNF hydrogel matrix. Ink with fluorescent dye was visualized under UV illumination. (c) It was possible to interconnect the layers by continuous injection of the ink in tip movement to the next layer. (d) CNF hydrogel matrix was dehydrated and formed a thin compact microfluidic film. (e) Printed ink was liquefied at elevated temperature and removed under vacuum, forming an open-channel 3D microfluidic device. (f) Different shapes of channel patterns formed in CNF films. Scale bars are 1 cm in (b) and (c) and 500 μm in (f).

potassium dichromate (Sigma-Aldrich) and nickel nitrate hexahydrate (Sigma-Aldrich) in DW were prepared, and calibration curves were obtained with UV−visible (UV−vis) spectroscopy for analysis of the ion concentrations. The mixture of ion solutions was injected into the inlet to evaluate the selectivity. The 10% H_2SO_4 and 1% NaOH solutions were eluted at the specific chelating condition of the metal ions, with dimethylglyoxime and 1,5-diphenylcarbazide at the detection zones. The flow rates of the heavy metal ion, H_2SO_4, and NaOH solutions were 50, 2, and 2 μL min^{-1}, respectively.

3. RESULTS AND DISCUSSION

Hydrophobic petroleum jelly was chosen as a counter ink material due to its immiscibility with the hydrophilic CNF hydrogel matrix and the ease of removal from the matrix after drying. The fabrication of microfluidic devices with multilayered channels in a film was achieved in three steps. The first step was to print the channels designed using CAD with a removable ink. The CNF suspension has a gel-like consistency above a concentration of 1.0% because CNFs are highly entangled (Figure S1a). A transmission electron microscopy (TEM) image of the air-dried CNF matrix showed that the fibrils had a width of approximately 10 nm (Figure S1b). As the nozzle moved through the CNF hydrogel matrix, the removable petroleum-jelly ink was printed inside the matrix (Figure 1a). The printing could be routinely performed, and three different shapes of channels were printed inside the matrix at different levels, which were interconnected through a junction between the layers (Figure 1b, c).

The second step was to dry the CNF hydrogel with printed features at room temperature. During the drying process, the CNF hydrogel matrix formed a condensed film structure that was still flexible (Figure 1d). The petroleum-jelly ink was stable over the drying process, and no leakage or damaged structure was observed. The third step was to remove the petroleum-jelly ink from the inside of the CNF films for the creation of channel structures. The petroleum-jelly ink started to liquefy above the melting point (>70 °C). This enabled the easy removal of the ink from the dried matrix and the formation of open-channel structures by flowing compressed air (Figure 1e). By using this facile method, various microfluidic channels such as straight lines, curves, intersections, and pockets could be fabricated (Figure 1f). Printed inks are fused at the meeting point of the printing nozzle at the same layer forming the intersections. The pocket designs could be introduced by positioning the needle during extrusion without *X*, *Y*, or *Z* translation. The pocket volumes could be easily controlled by adjusting the applied pressure or extrusion time.

Maintaining the detailed structure of the printed design was the most challenging part of liquid-based 3D printing. The viscosity of wood pulp increased rapidly from 27 to 150 Pa·s at a shear rate of 0.1 s^{-1} as it transformed into CNFs by mechanical grinding (Figure S2a). The storage modulus also increased after nanofibrillation of pulp cellulose proceeded and the gel-like property appeared (Figure S2b). This dramatic rheological change enabled CNFs, as a matrix material, to maintain the printed structures stably inside the matrix. Petroleum jelly was mixed with liquid paraffin to tailor its rheological properties and enhance its printability at room temperature. The viscosity of the petroleum-jelly-based ink was gradually decreased with an increased liquid paraffin ratio from 0 to 0.5, and the inks exhibited shear-thinning behavior, allowing them to be extruded through a fine deposition nozzle.

DOI: 10.1021/acsami.7b07609
ACS Appl. Mater. Interfaces XXXX, XXX, XXX−XXX

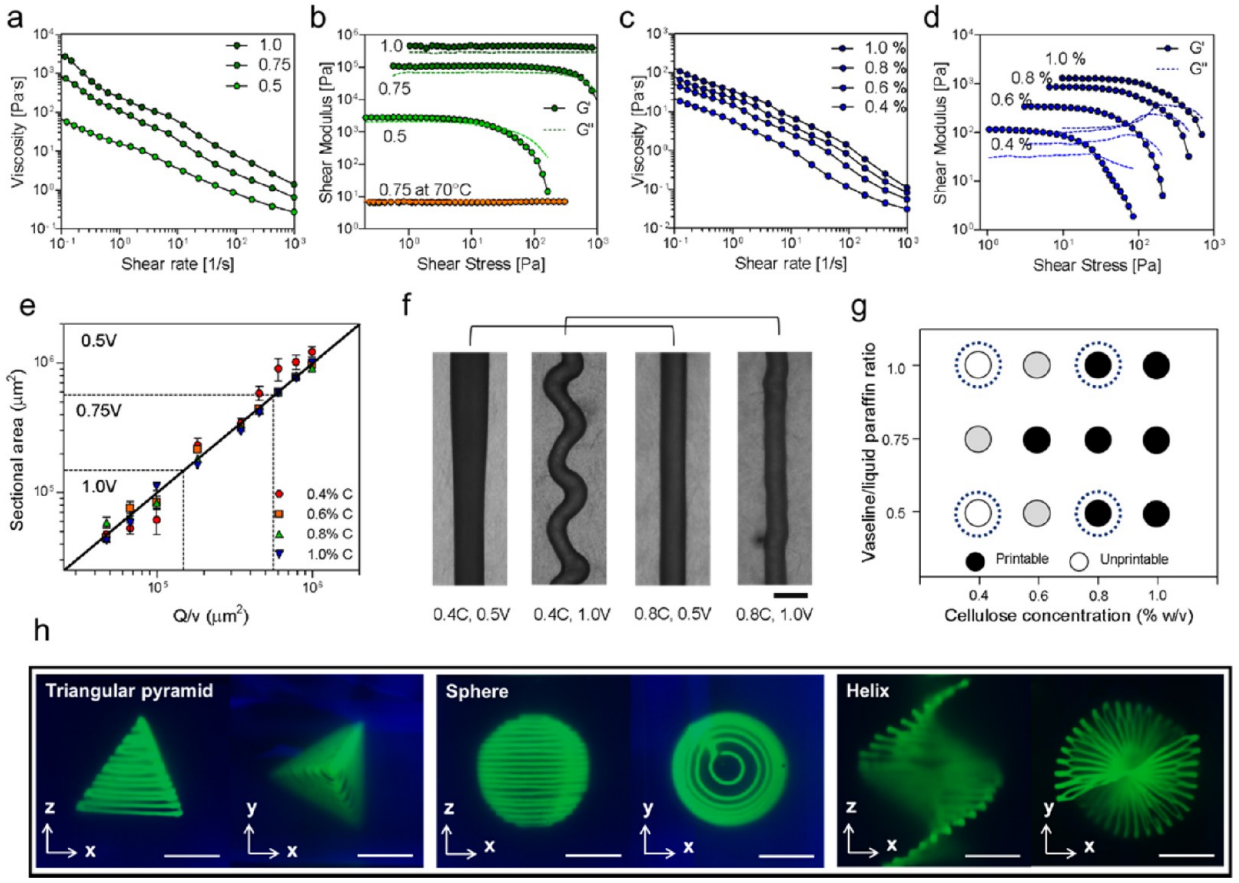

Figure 2. Free-standing 3D printing of petroleum-jelly ink in the CNF matrix. (a) Viscosity of petroleum-jelly ink as a function of shear rate. (b) Storage and loss moduli of petroleum-jelly ink as a function of shear stress. (c) Viscosity of the CNF hydrogel matrix as a function of shear rate. (d) Storage and loss moduli of the CNF hydrogel matrix as a function of shear stress. (e) Sectional area of printed paths at various material combinations. Ideal sectional area increases linearly with a slope of 1 at an increase of Q/v. (f) Optical microscopic images of printed paths at various conditions denoted in (g) as blue circles. (g) Printing performance at a variety of CNF matrix concentrations and ink composition ratios with printable (dark circles) and unprintable (light circles) combinations. (h) Creation of triangular pyramid, sphere, and helix structures with petroleum-jelly ink. The ink contains green fluorescent microspheres for illumination. The structures were imaged from the side and the top. Scale bars are 500 μm in (f) and 5 cm in (h).

Immediately after printing, the ink maintained its printed shape due to its gel-like property below the yield point ($G' > G''$) (Figure 2a, b). The matrix, a CNF hydrogel, played a role in keeping the printed structures in the bulk in a free-standing form. Since the rheological behavior of the CNF hydrogels was a critical factor, four different concentrations of CNF hydrogels were chosen, and their viscosity change was measured. The viscosity of the CNF hydrogels increased over the entire shear rate as the CNF concentration increased (Figure 2c). In addition, the storage modulus G' and the loss modulus G'' increased with increased CNF content in the matrix, as shown in Figure 2d.

Rheological optimization between the matrix and the ink materials was required to prevent the printed structures from changing their shapes. The surface tension and pressure-driven buckling of the ink material caused serious structural changes to the printed paths.[6] We investigated the cross-sectional areas printed at various CNF concentrations and the ink compositions using the petroleum jelly to liquid paraffin ratio (Figure 2e). The sectional area of the printed path usually exhibited ideal behavior over a wide range of flow rates, Q, and tip speeds, v, at various material combinations. However, the sectional area slightly deviated from an ideal trend at low concentrations of the CNF matrix used in the soft gels. The low viscosity of 0.5 V ink became thicker at the low concentration of the CNF matrix due to its contracting movement against the soft CNF matrix. In contrast, the high viscosity of 1.0 V ink showed low fluidity, and pressure-driven buckling was observed at the soft CNF matrix (Figure 2f, g). Fortunately, the instability of the printed inks was compensated by the use of a high concentration of CNF matrix, and the sectional area was close to the ideal value. Because of the increased matrix viscosity, the drag force acting opposite to the relative motion increased so that aggregation and buckling could be minimized. Diverse, more complex structures could be printed, including a triangular pyramid, a sphere, and a helix in a single pass (Figure 2h). The highly resolved structures were imaged by mixing fluorescent dye in the ink. The structures were sufficiently stable during printing and exhibited no significant changes after storage for approximately one month.

The CNF hydrogels formed a highly transparent film, and the transmittance was above 75% in the range of visible wavelengths in the film form (Figure S3a, b). The clarity of the CNF film was unique compared to that of normal cellulose paper used in analytical chemistry, with a potential enhanced efficiency for detection. The highly transparent substrates enabled the direct observation of the flowing channels rather than reflection from the paper surface. Channels were

DOI: 10.1021/acsami.7b07609
ACS Appl. Mater. Interfaces XXXX, XXX, XXX−XXX

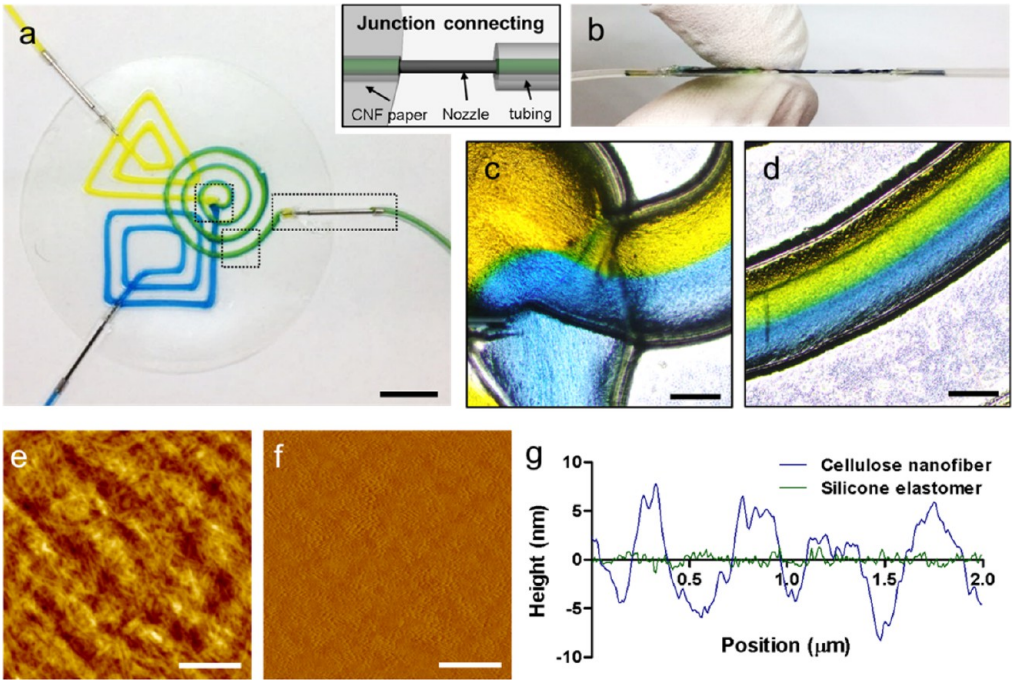

Figure 3. Feasibility test of microfluidic channel devices. (a) Injection of two dye solutions to two separate channels. Dye solutions were mixed at the circle-shaped channels and turned green. (b) Thickness of a CNF microfluidic device consisting of three layered channels located vertically. Optical images of the junction area (c) and laminar flow in the CNF microfluidic channels (d). Channel surface was coated with silicon elastomer to prevent water absorption. The fibrous channel surface (e) was modified into a smooth surface (f), and the surface roughness changed significantly after coating (g) and was confirmed by AFM. Scale bars are 1 cm in (a), 500 μm in (c) and (d), and 500 nm in (e) and (f).

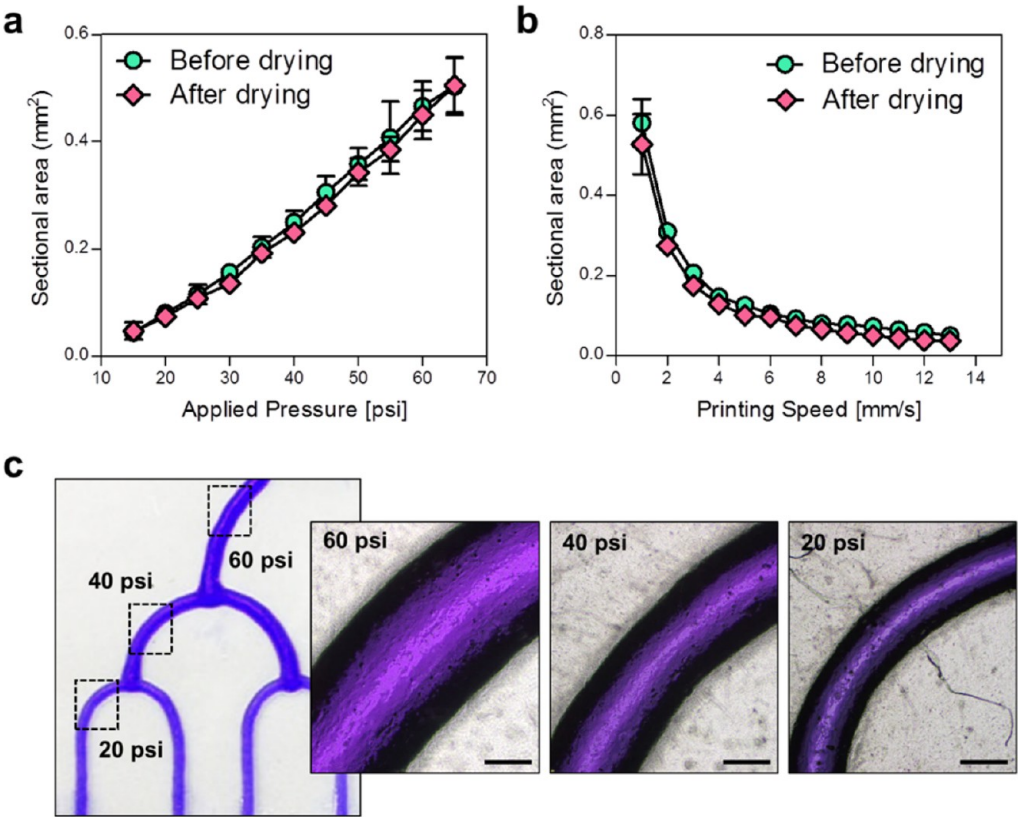

Figure 4. Control of channel diameters by pressure applied to the 3D-printing ink. Theoretical and experimental values of sectional areas of the microchannel were evaluated (a) as a function of applied pressure at a printing speed of 5 mm s^{-1} and (b) as a function of printing speed at an applied pressure of 25 psi using a 160 μm cylindrical stainless steel nozzle at 25 °C. (c) Channel size was controlled by simple adjustment of the applied pressure on the printed inks, which maintained their size after drying of the matrix. Scale bars are 500 μm in (c).

DOI: 10.1021/acsami.7b07609
ACS Appl. Mater. Interfaces XXXX, XXX, XXX−XXX

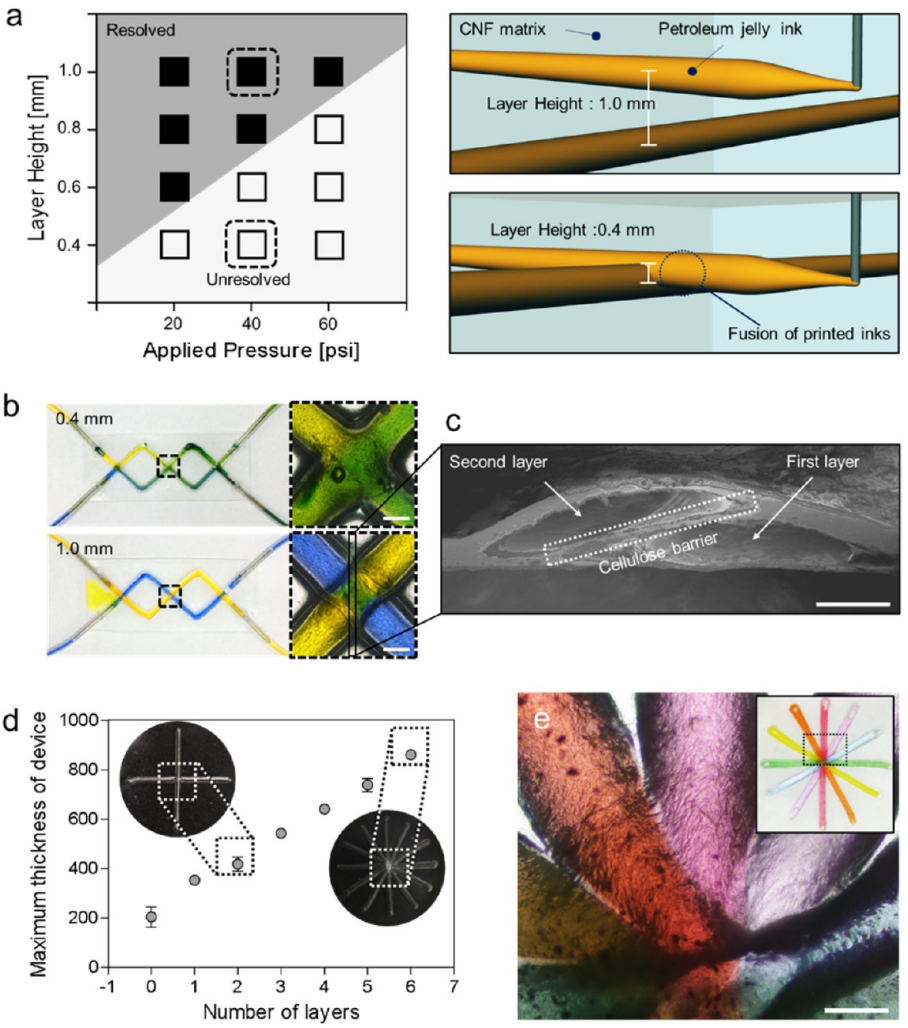

Figure 5. Dimension control of the microfluidic device. (a) Processing map for determining the dimension of the microfluidic devices, denoting regions resolved between the layers (filled-in squares) and unresolved between the layers (empty squares) as a function of the layer height between the nozzle tip and the applied pressure, with black boxes highlighting schematic illustration of the dimension control principle. At a certain applied pressure, when the distance between the layers is sufficient, the layers relocated separately. However, when the secondary printed layer was close to the previously printed layer, the printed inks fused, forming connected channels in the same layer. (b) Two different dye solutions flowed through the devices at different layer height conditions. (c) Detailed image of the cross-sectional 3D microfluidic devices showing the two channels blocked by a cellulose barrier. (d) Variation of the maximum thickness of the device depending on integration of the multilayered channels. (e) Photographs of six different solutions flowing in six layered microfluidic devices without mixing. Scale bars are 500 μm in (b) and (e) and 250 μm in (c).

connected to silicone tubing using a stainless steel bridge (Figure 3a). The thickness of a CNF microfluidic device consisted of three layered channels located vertically (Figure 3b). Two streams of aqueous dye solutions flowed through the separate microfluidic channels and met at a junction, making a laminar flow of the two streams through the CNF microfluidic channels (Figure 3c, d). We found that the CNF-based open-channel microfluidic devices could produce the same diffusion-limited coflows reported in conventional PDMS open-channel microfluidic devices (Figure 3d).[28,31] To prevent liquid penetration through the channel surface, the inside of the channel was coated with silicone elastomer (thickness: 26.33 ± 5.68 μm) (Figure S4). The fibrous structure of the channels disappeared, and a new nonporous surface was formed after the coating, inferring uniform coating of the surfaces (Figure 3e, f). The surface roughness was significantly reduced from RMS 4.09 nm to RMS 0.88 nm after the coating, confirming the effective coating of the CNFs with silicon elastomer (Figure 3g).

The elusion volume of the microchannels was closely related to the cross-sectional area of the channel, which was controlled by dynamic pressure variation from 10 to 60 psi in extruding the ink under the printing speed at 5 mm s^{-1}. The cross-sectional area of the channels was calculated by measuring the diameter of the extruded lines (Figure 4a, b). It was determined to increase linearly according to the applied pressure because of the larger amount of ink at the same time period under higher pressure (Figure 4c). A series of channels with different diameters could be fabricated by simple adjustment of the dynamic pressure during printing, as shown in Figure 4c.

Conventional paper-based open-channel microfluidic devices must be stacked to prepare 3D channel designs. In contrast, the proposed strategy here can control the positioning of the layers and their interconnection three-dimensionally through CAD design. The lower extruding dynamic pressure of the ink formed narrower structures, which required smaller spacing between the layers to resolve the structure (Figure 5a). Unless the minimum distance between the layers was not satisfied at a

DOI: 10.1021/acsami.7b07609
ACS Appl. Mater. Interfaces XXXX, XXX, XXX−XXX

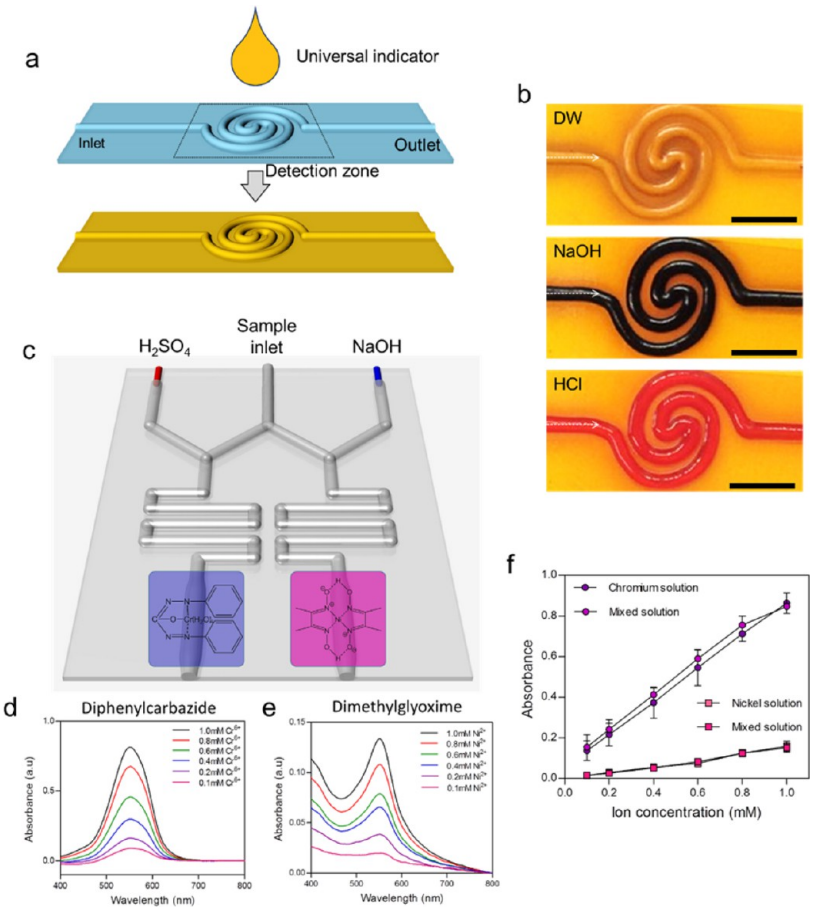

Figure 6. Colorimetric analysis of heavy metal ions in a dual mode. (a) Design of the detection zone of a CNF microfluidic device. A universal pH indicator solution was dropped at the surface of the detection zone and dried until use. (b) Streams of DW, 1 M NaOH, and 1 M HCl were injected into the device sequentially. Flows of NaOH caused a change in channel wall color to dark purple. Immediately after the flows of NaOH, flows of HCl caused a dramatic change in color to red. (c) Schematic drawing of the microfluidic device design for sensing heavy metal ions Ni^{2+} and Cr^{6+}. Dimethylglyoxime and diphenylcarbazide solutions were dropped on the outer surface of the optical windows on the devices. The mixed solution of heavy metal ions, the 10% H_2SO_4 solution, and the 1% NaOH solution were pumped at flow rates of 50, 2, and 2 μL min^{-1}, respectively. The heavy metal ion solution was mixed with either 10% H_2SO_4 or 1% NaOH solution at the separated channels, and the pH of each solution was adjusted for specific sensing of heavy metal ions. The dimethylglyoxime region changed color to pink by capture of Ni^{2+} under alkaline conditions. Meanwhile, the diphenylcarbazide region changed color to purple with capture of Cr^{6+} under acidic conditions. UV–vis spectra obtained at different concentrations of (d) potassium dichromate and (e) nickel nitrate hexahydrate for selective capture of heavy metal ions. Mixed solutions of potassium dichromate and nickel nitrate hexahydrate were used for the test. Absorbance increased linearly as a function of ion concentration. (f) Calibration curves for detection of Ni^{2+} and Cr^{6+} ions. Mixed solutions were analyzed at both detection zones and showed a close relationship with the calibration curves. Scale bars are 5 mm in (b).

certain applied pressure, the printed structures were merged, and the solutions were mixed at the fused region.

To examine the 3D microfluidic design, two different dye solutions flowed through the device (Figure 5b). The solutions flowed along the channels and mixed at the junction of the channels, turning green with a 0.4 mm spacing microfluidic design. Each solution flowed through the channel without mixing, with a 1.0 mm spacing microfluidic design; a dense CNF film barrier was formed in the middle of the channels during the drying process (Figure 5c). With the proposed matrix-assisted 3D-printing methods, it was possible to integrate the 3D channels. The thickness of the overlaid area increased linearly according to the number of channels used (Figure 5d). A total of six channels was overlaid in the investigation, and six colors of solution were injected into the channels separately. Amazingly, the open-channel microfluidic device delivered six solutions without mixing in the device, confirming well-resolved multilayer microfluidic devices less than 1 mm thick (Figure 5e).

The CNF film containing a network of interconnected pores generally exhibited higher permeability to liquids than the solid materials normally used to fabricate microfluidic devices. The closed detection systems using PDMS or other plastic-based microfluidic devices maintained the inertness with molecules during the flow. Meanwhile, a CNF-based microfluidic device allowed molecules to transport across the cellulose barrier, and the molecules were adsorbed at the channel surfaces as an open system. The open system had a variety of attractive features compared to the PDMS-based microfluidic devices. First, simple and active sensing was possible in a single channel line. Second, it was possible to integrate the open channels with a wicking zone through locational control of selective coatings.

The high water permeability of an uncoated CNF matrix was the key to the active colorimetric pH sensor. The transparency of the CNF channels enabled the detection of a color change

DOI: 10.1021/acsami.7b07609
ACS Appl. Mater. Interfaces XXXX, XXX, XXX–XXX

responding to the binding of molecules. The inside of the channels was coated with a silicon elastomer selectively, but the coiled region was left uncoated after the printing of the CNF-based microfluidic channels. A universal indicator was dropped in the coiled region for the detection of pH changes (Figure 6a). It was convenient to monitor the chemical changes occurring inside the channels according to acidity (Figure 6b). Flows of 1 M NaOH caused a color change in the channel to dark purple. Subsequently, the 1 M HCl solution caused a dramatic change in color to red. The device detects pH changes simply in real time without any sophisticated equipment.

The CNF-based platform is also applicable to monitoring heavy metals using pH-dependent reactions. The specific reaction between heavy metal ions and chemicals was considered at a certain pH condition, such as Ni^{2+} and dimethylglyoxime at pH 9 and Cr^{6+} and diphenylcarbazide at pH 1. For the feasibility of a device, a heavy metal solution was injected into the center inlet and mixed with buffer solutions of 10% H_2SO_4 and 1% NaOH injected into the different paths of the channels. The mixed solution reacted with either dimethylglyoxime or diphenylcarbazide in the detection zone (Figure 6c). Specifically, Ni^{2+} ions reacted with dimethylglyoxime under basic conditions, causing a colorimetric change to pink, and Cr^{6+} ions reacted with diphenylcarbazide under acidic conditions, causing a colorimetric change to purple. The changes in color in the monitoring zones were measured according to the metal ion concentration using UV−vis spectroscopy. The intensity of the peaks increased linearly as a function of the ion concentration (Figure 6d, e). The intensity of the absorbance increased linearly as the ion concentration increased. The mixed-ion solutions showed the same absorbances as the single-ion solutions, inferring the high selectivity of the device (Figure 6f).

4. CONCLUSIONS

The CNF is an ideal material for forming a hydrogel with suitable viscoelastic properties in 3D printing. We suggest CNF hydrogels as a 3D-structuring ultrathin film and a supporting matrix for 3D microchannels. The optimal combination of rheological properties between the CNF matrix and the petroleum ink enabled well-resolved 3D printing, and dehydration from the CNF hydrogel created an ultrathin film containing 3D structures. The filled-in inks were easily removed, and the selective coating of the inner channel surfaces was thus available. With the above-described features, a variety of complex structures can be 3D-printed in CNF hydrogels and designed for sensing platforms on a microfluidic basis.

Thus, 3D printing of CNF hydrogels solves critical issues in PDMS-based microfluidic devices such as flexibility and compactness. In addition, it overcomes the limitation in sample migration of wicking paper-based sensing platforms. This greater freedom in regional selectivity will broaden the potential application of 3D patterning in CNF hydrogels to novel areas.

The CNF hydrogel is a novel material for matrix-assisted 3D printing. The potential application of CNF hydrogels is much broader than described here. This novel route to creating 3D open-channel microfluidic devices based on CNFs is unique, and this is the first report to the best of our knowledge. Cellulose fibers are not only the most important resource in the paper industry but are also one of the most valuable materials in 3D printing.

ASSOCIATED CONTENT

Supporting Information

The Supporting Information is available free of charge on the ACS Publications website at DOI: 10.1021/acsami.7b07609.

Rheological properties of the CNF hydrogel before grinding carboxymethylated pulp cellulose and after grinding; morphologies of the grinded CNF under TEM and the gelling behavior of the CNF; optical transparency of the CNF thin films; fluorescent microscopic image of a silicone elastomer layer containing green fluorescent microparticles (PDF)

AUTHOR INFORMATION

Corresponding Author

*E-mail: jhyun@snu.ac.kr.

ORCID

Jinho Hyun: 0000-0002-9992-5681

Notes

The authors declare no competing financial interest.

ACKNOWLEDGMENTS

This research was supported by the Basic Science Research Program through the National Research Foundation of Korea (NRF) funded by the Ministry of Education (grant no. NRF-2015R1D1A1A01056711) and the Technology Innovation Program (grant no. 10062717, Development of Low-cost Mass Production Technology for Cellulose Nanofiber) funded by the Ministry of Trade, Industry & Energy (MOTIE, Korea).

REFERENCES

(1) Wu, W.; DeConinck, A.; Lewis, J. A. Omnidirectional Printing of 3D Microvascular Networks. *Adv. Mater.* **2011**, *23* (24), H178−H183.

(2) Kolesky, D. B.; Truby, R. L.; Gladman, A. S.; Busbee, T. A.; Homan, K. A.; Lewis, J. A. 3D Bioprinting of Vascularized, Heterogeneous Cell-Laden Tissue Constructs. *Adv. Mater.* **2014**, *26* (19), 3124−3130.

(3) Muth, J. T.; Vogt, D. M.; Truby, R. L.; Menguc, Y.; Kolesky, D. B.; Wood, R. J.; Lewis, J. A. Embedded 3D Printing of Strain Sensors within Highly Stretchable Elastomers. *Adv. Mater.* **2014**, *26* (36), 6307−6312.

(4) Parekh, D. P.; Ladd, C.; Panich, L.; Moussa, K.; Dickey, M. D. 3D Printing of Liquid Metals as Fugitive Inks for Fabrication of 3D Microfluidic Channels. *Lab Chip* **2016**, *16* (10), 1812−1820.

(5) Highley, C. B.; Rodell, C. B.; Burdick, J. A. Direct 3D Printing of Shear-Thinning Hydrogels into Self-Healing Hydrogels. *Adv. Mater.* **2015**, *27* (34), 5075−5079.

(6) Bhattacharjee, T.; Zehnder, S. M.; Rowe, K. G.; Jain, S.; Nixon, R. M.; Sawyer, W. G.; Angelini, T. E. Writing in the Granular Gel Medium. *Sci. Adv.* **2015**, *1* (8), e1500655.

(7) Habibi, Y.; Lucia, L. A.; Rojas, O. J. Cellulose Nanocrystals: Chemistry, Self-Assembly, and Applications. *Chem. Rev.* **2010**, *110* (6), 3479−3500.

(8) Beecher, J. F. Wood, Trees and Nanotechnology. *Nat. Nanotechnol.* **2007**, *2* (8), 466−467.

(9) Nogi, M.; Iwamoto, S.; Nakagaito, A. N.; Yano, H. Optically Transparent Nanofiber Paper. *Adv. Mater.* **2009**, *21* (16), 1595−1598.

(10) Koga, H.; Nogi, M.; Komoda, N.; Nge, T. T.; Sugahara, T.; Suganuma, K. Uniformly Connected Conductive Networks on Cellulose Nanofiber Paper for Transparent Paper Electronics. *NPG Asia Mater.* **2014**, *6* (3), e93.

(11) Fujisaki, Y.; Koga, H.; Nakajima, Y.; Nakata, M.; Tsuji, H.; Yamamoto, T.; Kurita, T.; Nogi, M.; Shimidzu, N. Transparent Nanopaper-Based Flexible Organic Thin-Film Transistor Array. *Adv. Funct. Mater.* **2014**, *24* (12), 1657−1663.

DOI: 10.1021/acsami.7b07609
ACS Appl. Mater. Interfaces XXXX, XXX, XXX−XXX

(12) Isogai, A.; Saito, T.; Fukuzumi, H. TEMPO-oxidized Cellulose Nanofibers. *Nanoscale* **2011**, *3* (1), 71−85.
(13) Ghaderi, M.; Mousavi, M.; Yousefi, H.; Labbafi, M. All-cellulose Nanocomposite Film Made from Bagasse Cellulose Nanofibers for Food Packaging Application. *Carbohydr. Polym.* **2014**, *104*, 59−65.
(14) Domingues, R. M. A.; Chiera, S.; Gershovich, P.; Motta, A.; Reis, R. L.; Gomes, M. E. Enhancing the Biomechanical Performance of Anisotropic Nanofibrous Scaffolds in Tendon Tissue Engineering: Reinforcement with Cellulose Nanocrystals. *Adv. Healthcare Mater.* **2016**, *5* (11), 1364−1375.
(15) Zhou, C. J.; Shi, Q. F.; Guo, W. H.; Terrell, L.; Qureshi, A. T.; Hayes, D. J.; Wu, Q. L. Electrospun Bio-Nanocomposite Scaffolds for Bone Tissue Engineering by Cellulose Nanocrystals Reinforcing Maleic Anhydride Grafted PLA. *ACS Appl. Mater. Interfaces* **2013**, *5* (9), 3847−3854.
(16) He, X.; Xiao, Q.; Lu, C. H.; Wang, Y. R.; Zhang, X. F.; Zhao, J. Q.; Zhang, W.; Zhang, X. M.; Deng, Y. L. Uniaxially Aligned Electrospun All-Cellulose Nanocomposite Nanofibers Reinforced with Cellulose Nanocrystals: Scaffold for Tissue Engineering. *Biomacromolecules* **2014**, *15* (2), 618−627.
(17) Olsson, R. T.; Azizi Samir, M. A. S.; Salazar-Alvarez, G.; Belova, L.; Strom, V.; Berglund, L. A.; Ikkala, O.; Nogues, J.; Gedde, U. W. Making Flexible Magnetic Aerogels and Stiff Magnetic Nanopaper Using Cellulose Nanofibrils as Templates. *Nat. Nanotechnol.* **2010**, *5* (8), 584−588.
(18) Wang, M.; Anoshkin, I. V.; Nasibulin, A. G.; Korhonen, J. T.; Seitsonen, J.; Pere, J.; Kauppinen, E. I.; Ras, R. H. A.; Ikkala, O. Modifying Native Nanocellulose Aerogels with Carbon Nanotubes for Mechanoresponsive Conductivity and Pressure Sensing. *Adv. Mater.* **2013**, *25* (17), 2428−2432.
(19) Shi, Z. Q.; Gao, H. C.; Feng, J.; Ding, B. B.; Cao, X. D.; Kuga, S.; Wang, Y. J.; Zhang, L. N.; Cai, J. In Situ Synthesis of Robust Conductive Cellulose/Polypyrrole Composite Aerogels and Their Potential Application in Nerve Regeneration. *Angew. Chem., Int. Ed.* **2014**, *53* (21), 5380−5384.
(20) Wang, B.; Li, X. L.; Luo, B.; Yang, J. X.; Wang, X. J.; Song, Q.; Chen, S. Y.; Zhi, L. J. Pyrolyzed Bacterial Cellulose: A Versatile Support for Lithium Ion Battery Anode Materials. *Small* **2013**, *9* (14), 2399−2404.
(21) Nystrom, G.; Razaq, A.; Stromme, M.; Nyholm, L.; Mihranyan, A. Ultrafast All-Polymer Paper-Based Batteries. *Nano Lett.* **2009**, *9* (10), 3635−3639.
(22) Chen, L. F.; Huang, Z. H.; Liang, H. W.; Guan, Q. F.; Yu, S. H. Bacterial-Cellulose-Derived Carbon Nanofiber@MnO2 and Nitrogen-Doped Carbon Nanofiber Electrode Materials: An Asymmetric Supercapacitor with High Energy and Power Density. *Adv. Mater.* **2013**, *25* (34), 4746−4752.
(23) Siqueira, G.; Kokkinis, D.; Libanori, R.; Hausmann, M. K.; Gladman, A. S.; Neels, A.; Tingaut, P.; Zimmermann, T.; Lewis, J. A.; Studart, A. R. Cellulose Nanocrystal Inks for 3D Printing of Textured Cellular Architectures. *Adv. Funct. Mater.* **2017**, *27* (12), 1604619.
(24) Markstedt, K.; Mantas, A.; Tournier, I.; Martínez Ávila, H.; Hagg, D.; Gatenholm, P. 3D Bioprinting Human Chondrocytes with Nanocellulose-Alginate Bioink for Cartilage Tissue Engineering Applications. *Biomacromolecules* **2015**, *16* (5), 1489−1496.
(25) Sydney Gladman, A.; Matsumoto, E. A.; Nuzzo, R. G.; Mahadevan, L.; Lewis, J. A. Biomimetic 4D Printing. *Nat. Mater.* **2016**, *15* (4), 413−418.
(26) Torres-Rendon, J. G.; Femmer, T.; De Laporte, L.; Tigges, T.; Rahimi, K.; Gremse, F.; Zafarnia, S.; Lederle, W.; Ifuku, S.; Wessling, M.; Hardy, J. G.; Walther, A. Bioactive Gyroid Scaffolds Formed by Sacrificial Templating of Nanocellulose and Nanochitin Hydrogels as Instructive Platforms for Biomimetic Tissue Engineering. *Adv. Mater.* **2015**, *27* (19), 2989−2995.
(27) Li, X.; Ballerini, D. R.; Shen, W. A Perspective on Paper-based Microfluidics: Current Status and Future Trends. *Biomicrofluidics* **2012**, *6* (1), 011301.
(28) Glavan, A. C.; Martinez, R. V.; Maxwell, E. J.; Subramaniam, A. B.; Nunes, R. M. D.; Soh, S.; Whitesides, G. M. Rapid Fabrication of Pressure-driven Open-channel Microfluidic Devices in Omniphobic R-F Paper. *Lab Chip* **2013**, *13* (15), 2922−2930.
(29) Thuo, M. M.; Martinez, R. V.; Lan, W. J.; Liu, X. Y.; Barber, J.; Atkinson, M. B. J.; Bandarage, D.; Bloch, J. F.; Whitesides, G. M. Fabrication of Low-Cost Paper-Based Microfluidic Devices by Embossing or Cut-and-Stack Methods. *Chem. Mater.* **2014**, *26* (14), 4230−4237.
(30) Hamedi, M. M.; Unal, B.; Kerr, E.; Glavan, A. C.; Fernandez-Abedul, M. T.; Whitesides, G. M. Coated and Uncoated Cellophane as Materials for Microplates and Open-channel Microfluidics Devices. *Lab Chip* **2016**, *16* (20), 3885−3897.
(31) Ismagilov, R. F.; Stroock, A. D.; Kenis, P. J. A.; Whitesides, G.; Stone, H. A. Experimental and Theoretical Scaling Laws for Transverse Diffusive Broadening in Two-phase Laminar Flows in Microchannels. *Appl. Phys. Lett.* **2000**, *76* (17), 2376−2378.

DOI: 10.1021/acsami.7b07609
ACS Appl. Mater. Interfaces XXXX, XXX, XXX−XXX